Optimal Design of a High Speed SPM Motor for Machine Tool Applications

Chang-Chou Hwang[1], San-Shan Hung[2], Cheng-Tsung Liu[3], and Shih-Ping Cheng[4]

[1]Department of Electrical Engineering, Feng Chia University, Taichung 407, Taiwan
[2]Department of Automatic Control Engineering, Feng Chia University, Taichung 407, Taiwan
[3]Department of Electrical Engineering, National Sun Yat-sen University, Kaohsiung 804, Taiwan
[4]Department of Electrical Engineering, Nan Kai University of Technology, Nantou 542, Taiwan

This paper deals with the optimal design of surface-mounted permanent magnet motors for use in a high speed spindle machine tool in glass grinding applications. We apply the Taguchi method to refine the stator structure and use segmented rotor magnets for the motor to yield the desired performance. A thermal analysis is conducted to obtain the temperature distribution within the motor. We examine the results using finite element analysis and validate them by experimental measurements.

***Index Terms*—Efficiency, finite element analysis (FEA), surface-mounted permanent magnet (SPM) motor, Taguchi method, torque ripple.**

I. Introduction

HIGH-SPEED brushless permanent magnet (PM) motors have been widely used in many industry applications such as machine tools, compressors, vacuum pumps, and friction welding units due to their high efficiency and power density, small size, and low weight [1]–[3]. There are several possible PM motor designs for high-speed operations: 2-pole [1]–[4], [6]–[8] or 4-pole [5], [9]; 3-slot [1], [4], [6] or 6-slot [5], [9]; overlapping [2], [3], [5] or nonoverlapping [1], [5], [9] windings; slotted [1]–[9] or slotless [6]–[8] stators; and rotors with [3], [9] or without [1], [2], [4]–[8] a sleeve retaining the surface-mounted magnets.

By making comparisons of all possible designs, a 3-phase, 2-pole with a retaining sleeve, 3-slot with nonoverlapping windings stator SPM motor has been chosen in this paper for glass grinding. In this application, the motor was designed to provide high efficiency and low torque ripple with minimal package size and weight. The Taguchi parameter method coupled with finite element analysis (FEA) was employed to maximize the efficiency and minimize the torque ripple of the motor [10]–[12].

Aside from the electromagnetic design considerations described in this paper, thermal design is also important, especially for motors with high speed operation. Traditionally, thermal studies of electrical motors have been carried out by analytical techniques or numerical methods, such as thermal network [13], finite difference and finite element methods [14], [15]. In this paper, the lumped circuit models are conducted to assess the rated operation condition and thermal behavior of the motor [16]. Finally, a prototype machine was fabricated and tested to confirm the simulation results. They revealed good agreement.

II. Initial Design of Motor

The motor is rated at a power of 1500 W, rotating at 60 000 r/min. The initial design of the motor consists of a stator having three slots which carry nonoverlapping windings, and a 2-pole diametrically magnetized sintered NdFeB magnet rotor with a carbon fiber sleeve as shown in Fig. 1 and Table I. The 2-pole rotor consists of a unique cylindrical piece of magnet and a shaft. The magnet has a remanence of 1.2 T and a relative recoil permeability of 1.05. Since the ratio of the slot opening to slot pitch is low, the losses induced from the stator slotting permeance harmonics are generally quite small [17]. Therefore, rather than using laminations, the rotor yoke uses a magnet solid steel, such as alloy ID 35 CD 4 [18].

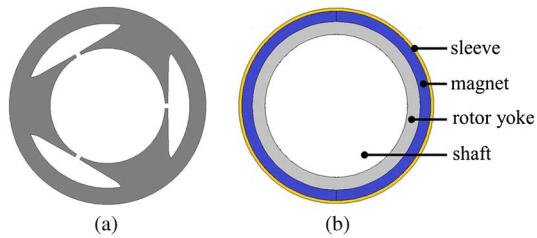

Fig. 1. Initial design of the motor topology. (a) Three-slot stator. (b) Two-pole rotor.

TABLE I
Initial Design of Motor Specifications

Specification	Dimension
Shaft outer diameter [mm]	19
Rotor yoke thickness [mm]	1.7
Magnet thickness [mm]	1.4
Sleeve thickness [mm]	0.4
Air gap length [mm]	1
Stator inner & outer diameter [mm]	28 & 48
Stack length [mm]	45

The losses of the motor include iron losses in the stator, copper losses in the winding, eddy current losses in the rotor, and rotational losses due to friction and windage. It is well known that the iron losses are the dominant contributor in a high speed machine [5]–[8]. The total iron losses P_{iron} can be obtained from (1) and (2) [12] as follows:

$$dp_{\mathrm{iron}} = \left[\mathrm{k_h B_m^2 f} + \frac{\pi^2 \sigma \mathrm{d}^2}{6} (\mathrm{B_m f})^2 + \mathrm{k_e (B_m f)^{3/2}} \times 8.67 \right] \mathrm{k_f} \quad (1)$$

$$P_{\mathrm{iron}} = \int \mathrm{dP_{iron} dv} \quad (2)$$

Manuscript received April 22, 2013; revised July 25, 2013; accepted July 26, 2013. Date of current version December 23, 2013. Corresponding author: C.-C. Hwang (e-mail: cchwang@fcu.edu.tw).

Color versions of one or more of the figures in this paper are available online at http://ieeexplore.ieee.org.

Digital Object Identifier 10.1109/TMAG.2013.2276092

TABLE II
PARAMETERS OF STATOR IRON

Item	Symbol	Value
Frequency [Hz]	f	1000
Electrical conductivity [S/m]	σ	2127660
Lamination thickness [mm]	d	0.35
Stacking factor	k_f	0.94
Hysteresis loss coefficient [Ws/T^2m^3]	k_h	126.188
Eddy current loss coefficient [$W/((T/s)^{1.5}m^3)$]	k_e	0.35052

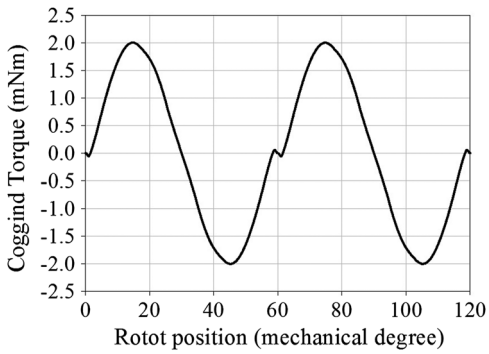

Fig. 2. Cogging torque versus rotor position.

TABLE III
INITIAL DESIGN OF MOTOR PERFORMANCE

Parameter	Symbol	Value
Output power [W]	P_{out}	1573.75
Average torque [Nm]	T_{avg}	0.251
Cogging torque [mNm]	T_{cog}	4.009
Torque ripple [%]	T_{rip}	8.06
Stator iron loss [W]	P_{iron}	104.54
Copper loss [W]	P_{cop}	22.21
Eddy current loss [W]	P_{edd}	63.25
Total loss [W]	P_{tot}	190.03
Efficiency [%]	η	88.55

where f and B_m are the frequency and amplitude of the fundamental flux density, σ is the electrical conductivity, d is the lamination thickness, and k_f is the iron stacking factor, k_h and k_e are the hysteresis loss coefficient and eddy current loss coefficient of the stator iron material. The stator uses Fe–Si laminations with a thickness of 0.35 mm and a saturated flux of 1.7 T. Table II gives the loss coefficients for the iron loss prediction. The eddy current losses in the magnets can be also calculated at 60 000 r/min using the *Flux2D* software package [12]. The NdFeB magnet has a resistivity of $1.44 \times 10^{-6}\Omega \cdot m$ at 20°C.

The machine performance can be predicted using FEA simulation as shown in Table III. In the Table, T_{rip} is the peak-to-peak values of torque ripple divided by average torque. It can be observed from Table III that the motor meets the output power requirement of 1500 W. However, the efficiency is lower and the torque ripple is higher. Fig. 2 shows the cogging torque curve versus rotor position. The peak-to-peak value of cogging torque is 4.009 mNm. It is about 1.6% of the rated average torque of 0.251 Nm in the initial design. The net radial force is small, and the permanent magnet is encased in a sleeve. Therefore, in this application, net radial force has little impact on performance.

TABLE IV
PARAMETERS DEFINITIONS AND DESIGN LEVEL CLASSIFICATION

Factor	Definition	Level 1	Level 2	Level 3
A	Stator teeth width [mm]	13	14	15
B	Stator yoke width [mm]	3.5	4	4.5
C	Air gap length [mm]	0.9	1	1.1
D	Slot opening [mm]	1.2	1.3	1.4

The underlined number indicates the initial design value.

TABLE V
MOTOR PERFORMANCE

Experiment	T_{rip} [%]	η [%]
1	22.46	88.65
2	21.85	89.355
3	3.09	90.445
4	19.04	88.96
5	6.79	89.90
6	4.35	90.10
7	15.96	89.37
8	10.405	89.65
9	3.56	90.41

III. PERFORMANCE IMPROVEMENT

A. Optimal Refinement of Stator Structure

Since the initial design configuration has high iron losses, the first-step to improve performance is therefore to refine the stator structure using the Taguchi method.

1) Taguchi Methodology: By adopting the Taguchi method, four factors, A, B, C, and D, corresponding to four design variables, are chosen as shown in Fig. 3, and each at three levels. The optimal factor-level combination of those factors as listed in Table IV can be systematically derived. The performance of the machine in the $L_9(3^4)$ matrix experiments can then be obtained from 2-D FEA, as shown in Table V.

2) Experiment Conduction: The influence of each factor on the torque ripple and efficiency is shown in Fig. 4. It can be seen that factor-level combinations (A3, B3, C3, and D3) help to both the minimization of torque ripple and the maximization of efficiency.

3) Results Analysis: The performance of the optimized machine was obtained using FEA simulation. Table VI compares the data of the machine between the initial design and the Taguchi method. It can be seen that the torque ripple reduces from the initial design of 8.06% to the Taguchi method of 3.02%, and the efficiency increases from the initial design of 88.85% to the Taguchi method of 90.41%. However, the copper losses increase slightly. This is because the stator teeth and yoke widths increase from the initial design of 14 and 4 mm to the Taguchi method of 15 and 4.5 mm, respectively. As a result, the slot cross-sectional area available for windings decreases, and consequently the current density and copper losses increase. It is noted that the refinement of the stator structure can improve the machine performance, however, the rotor eddy current losses reduce very slightly. Therefore, a method to reduce the rotor eddy current losses is adopted in the following study.

TABLE VI
MOTOR PERFORMANCE

Parameter	Initial	Taguchi
P_{out} [W]	1573.75	1701.68
T_{avg} [Nm]	0.251	0.271
T_{cog} [mNm]	4.009	0.58
T_{rip} [%]	8.06	3.02
P_{iron} [W]	104.54	84.17
P_{cop} [W]	22.21	25.5
P_{edd} [W]	63.25	61.95
P_{tot} [W]	190.03	171.62
η [%]	88.55	90.41

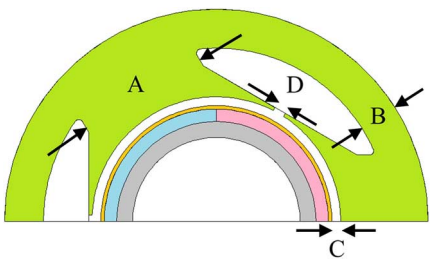

Fig. 3. Definition of factors.

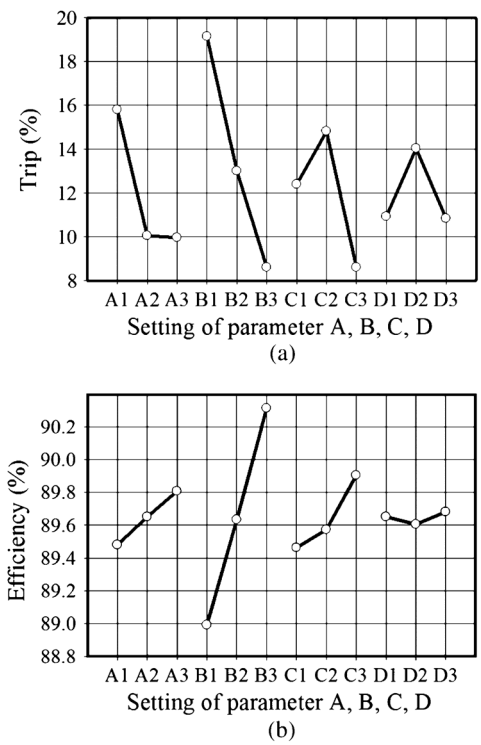

Fig. 4. Main factor effects on (a) torque ripple and (b) efficiency.

B. Method of Reducing Rotor Eddy Current Losses

The most straightforward way to limit rotor eddy current losses is to increase the resistivity of the magnets. Here each rotor pole magnet is divided into several segments (SEGs) along the circumference of the rotor, as shown in Fig. 5 [17].

Fig. 6 shows the variation of rotor eddy current losses and efficiency with rotor segments. As the number of rotor segment increases, the rotor eddy current losses decrease and the efficiency increases. To ease manufacture, each magnet pole is segmented into six pieces and the size of one piece is 6.8 mm $\times$ 1.4 mm $\times$ 45 mm. It is suitable and easy for locking between the block and rotor yoke in the manufacturing process. Table VII gives the effects of segmentation on machine performance. By segmenting the magnet, the rotor eddy current losses should be reduced. However, other losses are not significantly affected. These simulations confirm that the technique is effective in reducing the rotor eddy-current losses, and therefore in increasing overall machine efficiency. Here six segments are chosen. Fig. 7 shows the photographs of the prototype motor. Fig. 8 compares the torque curves. It shows good agreement between the calculated and the measured torque and torque ripple.

In summary, the torque ripple reduces from the initial design of 8.06%, to the Taguchi method of 3.02%, to the final result of 2.76%, while the efficiency increases from the initial design of 88.85%, to the Taguchi method of 90.41%, to the final result of 93.28%. The output power also increases about 200 W and meets the required specifications.

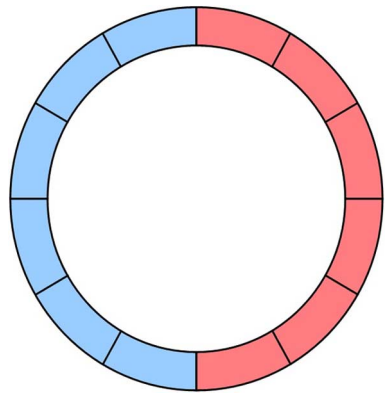

Fig. 5. Rotor with six segmented magnets per pole.

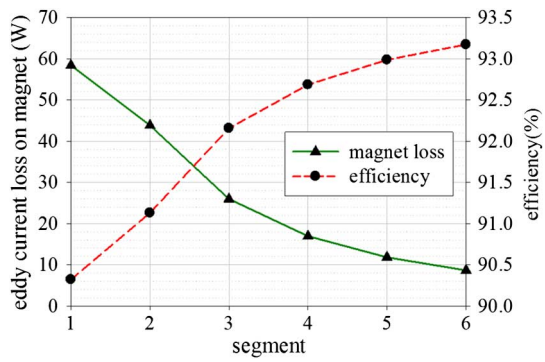

Fig. 6. Variation of P_{edd} and η with the rotor segments.

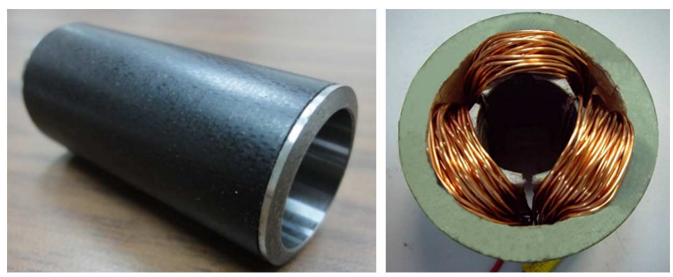

Fig. 7. Photographs of the realized prototype. (a) Rotor using carbon fiber sleeve. (b) Stator with nonoverlapping windings.

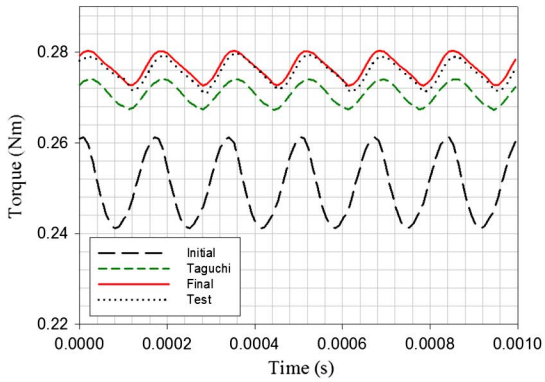

Fig. 8. Comparison of torque curves.

TABLE VII
PERFORMANCE COMPARISON

SEG	T_{avg} [Nm]	T_{rip} [%]	P_{out} [W]	P_{cdd} [W]	P_{iron} [W]	η [%]
1	0.271	3.02	1701.68	61.95	84.17	90.41
2	0.273	4.61	1715.30	41.37	83.75	91.55
3	0.275	1.55	1726.01	26.43	83.62	92.35
4	0.276	2.89	1732.07	18.29	83.49	92.83
5	0.2766	2.72	1735.76	13.30	83.42	93.11
6	0.277	2.76	1738.08	10.31	83.37	93.28

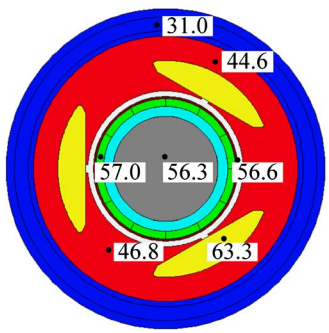

Fig. 9. Temperatures for some typical positions within the cross-section of the motor.

IV. THERMAL ANALYSIS

In this study, the lumped parameter thermal model is carried out using the *Motor-CAD* software package to assess the rated operation condition and thermal behavior of the motor [16]. To reduce the temperature rise, the prototypes of the motor use a closed, forced fluid cooling system using constant temperature emulsified water. The water flows at the rated value of 0.6 L/m inside the chamber that spiral surrounds the stator. The temperature of inlet water is set at 30 °C. Based on the losses obtained in the previous sections, temperatures for some typical positions within the motor, operating at the rated operation condition, are plotted in Figs. 9 and 10. It can be seen that the normal operating temperature of motor is below critical temperature.

V. CONCLUSION

This paper has presented an SPM machine topology suitable for use in a high speed spindle machine tool. The proposed refinements to the stator can improve the machine performance and the rotor magnet segmentation can further improve the efficiency of the motor. A thermal analysis confirmed that the temperature distribution within the motor was below critical temperature.

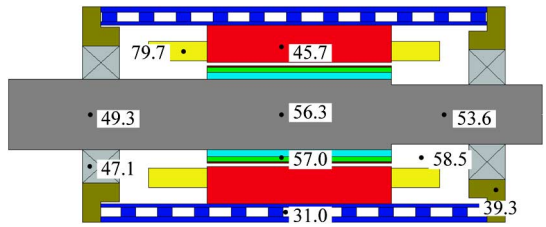

Fig. 10. Temperatures for some typical positions along the axial of the motor.

ACKNOWLEDGMENT

This work was supported by the National Science Council of Taiwan under Grant NSC 99-2221-E-035-101-MY3.

REFERENCES

[1] D. E. Hesmondhalgh, D. Tipping, and M. Amrani, "Design and construction of a high-speed high-performance direct-drive handpiece," *IEEE Proc.*, vol. 134 Pt. B, no. 6, pp. 286–296, Nov. 1987.
[2] F. Dubas, C. Espanet, and A. Miraoui, "Design of a high-speed permanent magnet motor for the drive of a fuel cell air-compressor," in *Proc. 2005 IEEE Conf. Vehicle Power and Propulsion*, Sep. 7–9, , pp. 603–610.
[3] S. M. Jang, H. W. Cho, and S. K. Choi, "Design and analysis of a high-speed brushless DC motor for centrifugal compressor," *IEEE Trans. Magn.*, vol. 43, no. 6, pp. 2573–2575, Jun. 2007.
[4] Z. Q. Zhu, K. Ng, and D. Howe, "Design and analysis of high-speed brushless permanent magnet motors," in *Proc. IEEE Electric Machines and Drive Conf.*, Sep. 1-3, 1997, vol. EMD97, pp. 381–385.
[5] Y. Pang, Z. Q. Zhu, and D. Howe, "Analytical determination of optimal split ratio for permanent magnet brushless motors," *IEEE Proc.-Electr. Power Appl.*, vol. 153, no. 1, pp. 7–13, Jan. 2006.
[6] N. Bianchi, S. Bolognani, and F. Luise, "Potentials and limits of high-speed PM motors," *IEEE Trans. Ind. Appl.*, vol. 40, no. 6, pp. 1570–1578, Nov./Dec. 2004.
[7] N. Bianchi, S. Bolognani, and F. Luise, "Analysis and design of a PM brushless motors for high speed operations," *IEEE Trans. Energy Convers.*, vol. 20, no. 3, pp. 629–637, Sep. 2005.
[8] N. Bianchi, S. Bolognani, and F. Luise, "High speed drive using a slotless PM motor," *IEEE Trans. Power Electron.*, vol. 21, no. 4, pp. 1083–1090, Jul. 2006.
[9] F. Zhou, J. Shen, W. Fei, and R. Lin, "Study of retaining sleeve and conductive shield and their influence on rotor loss in high speed PM BLDC motors," *IEEE Trans. Magn.*, vol. 42, no. 10, pp. 3398–3400, Oct. 2006.
[10] C. C. Hwang, L. Y. Lye, C. T. Liu, and P. L. Li, "Optimal design of an SPM motor using genetic algorithms coupled Taguchi method," *IEEE Trans. Magn.*, vol. 44, no. 11, pp. 4325–4328, Nov. 2008.
[11] R. K. Roy, *Design of Experiments Using the Taguchi Approach*. New York, NY, USA: Wiley, 2001.
[12] Flux User's Guide ver. 10.4.2, Magsoft Corporation. Ballston Spa. New York, NY, USA, 2011.
[13] T. J. Roberts, "The solution of the heat flow equations in large electrical machines," in *Proc. Instn. Mech. Engr.*, 1969-1970, vol. pt. 3E184, pp. 70–83.
[14] K. Reichert, "The calculation of the temperature distribution in electrical machines with the aid of the finite difference method," *Elektro Tech Z-A*, 1969, Bd 90, H6.
[15] C. C. Hwang, S. S. Wu, and Y. H. Jiang, "Novel approach to the solution of temperature distribution in the stator of an induction motor," *IEEE Trans. Energy Convers.*, vol. 15, no. 4, pp. 401–406, Dec. 2000.
[16] Motor-CAD User's Guide, Ver. 7.1.7.1, Motor Design Ltd., UK,, 2012.
[17] J. R. Hendershot, Jr. and T. J. E. Miller, *Design of Brushless Permanent-Magnet Machines*: Motor Design Books LLC, 2010.
[18] AFNOR 35 CD 4 Steel [Online]. Available: http://www.Steelss.com/Alloy/afnor-35-cd-4.html/, 2013/07/24